Velocity map imaging of the dynamics of bimolecular chemical reactions

S.J. Greaves, R.A. Rose and A.J. Orr-Ewing*

School of Chemistry, University of Bristol, Cantock's Close, Bristol BS8 1TS, UK

19 January 2010

Figures: 10

Tables: 0

* Author for correspondence

e-mail: a.orr-ewing@bris.ac.uk

Abstract

The experimental technique of velocity map imaging (VMI) enables measurements to be made of the dynamics of chemical reactions that are providing unprecedented insights about reactive scattering. This perspective article illustrates how VMI, in combination with crossed-molecular beam, dual-beam or photo-initiated (PHOTOLOC) methods, can reveal correlated information on the vibrational quantum states populated in the two products of a reaction, and the angular scattering of products (the differential cross section) formed in specific rotational and vibrational levels. Reactions studied by VMI techniques are being extended to those of polyatomic molecules or radicals, and of molecular ions. Subtle quantum-mechanical effects in bimolecular reactions can provide distinct signatures in the velocity map images, and are exemplified here by non-adiabatic dynamics on coupled potential energy surfaces, and by experimental evidence for scattering resonances.

1. Introduction

Much of the chemical change that occurs in the laboratory or the surrounding environment is caused by collisions between atoms, radicals, molecules or ions. To understand chemistry at a fundamental level, whether in solution (perhaps in a synthetic organic chemical reaction), at an interface (such as in heterogeneous catalysis), in the gas phase (for example, in the atmosphere of Earth or other planets, or at the ultralow temperatures of interstellar space) or in plasmas (such as those used for materials processing), we need quantitative descriptions of the rates and mechanisms of reactive collisions. Among many important parameters affecting reactivity, these descriptions might include the dependence of the reaction on the energy of the collision, the orientations of the reagents (i.e., the stereochemistry), and the electronic states of the participating species.[1,2] The electronic configurations of the reactants are particularly important because changes in the bonding or anti-bonding interactions determine the overall energy change from reagents to products and the locations of any energy barriers or wells along the reaction path. The variation in the potential energy with changes in the positions of all the atoms of the colliding species defines a multi-dimensional potential energy surface (PES), which is a key component of our understanding of chemical reactions. The PES controls the motions of all the atoms involved in a reaction because the forces experienced by the atoms at any particular geometrical configuration are determined by the gradients of the PES at that configuration. The shape of the PES incorporates the dependence of energy barrier heights or well depths on molecular geometry (such as relative orientation, or extension, compression and bending motions of certain bonds) and therefore determines whether a collision succeeds or fails to cause a chemical reaction. It also influences how the available energy is partitioned between different degrees of freedom of the products, namely vibrational modes (of which there can be many for polyatomic species; some modes may be more favoured than others), and translation and rotational motions.

Modern electronic structure calculation methods provide a means to quantify electronic energies for different geometries of a molecular system, and therefore can, in principle, be used to compute an array of energy points at selected geometries from which a PES is constructed. *Ab initio* calculations, which do not incorporate any empirical information, are proving increasingly successful for stable molecules or reactive systems involving a small number of light atoms with few electrons.[3-6] For heavier atoms, the greater number of electrons increases the computational burden, while including more atoms raises the number of dimensions needed for a full PES (for *N*

atoms, 3*N* – 6 dimensions are required to specify the arrangements of all the atoms). For computational expediency, approximations are therefore required to obtain PESs for all but a few select chemical reaction: these approximations include use of semi-empirical functions describing the potential energy;[7] reduced dimensionality calculations,[8] in which only a limited number of degrees of freedom considered important to understand the reaction pathway are considered explicitly; or calculation of PE values "on-the-fly" only at geometries required for a computer simulation of the reaction.[9] Calculations of the nuclear dynamics then provide a bridge to experimental studies of chemical reaction mechanisms because they simulate the motions that take colliding species over any energy barriers, and show how the energy available to the products is channelled into vibrational, rotational and translational motions – properties of the products that can be measured by the modern arsenal of experimental techniques based on molecular beam and laser spectroscopy methods.[10,11] Complementary experimental measurements can thus provide critical tests of the accuracy of a PES, and can be used to refine the choice of method used in an *ab initio* calculation, or to assess the validity of a semi-empirical electronic structure calculation method or the neglect of some degrees of freedom in a reduced-dimensionality treatment. For a given PE function, the calculation of the nuclear dynamics is, itself, a challenging task. Quantum dynamics may be treated using either time independent or time-dependent (wavepacket) scattering methods,[12] but only for a limited number of degrees of freedom. Classical trajectory methods provide a tractable and fast alternative to QM scattering calculations but will not account correctly for various quantum-mechanical phenomena such as tunnelling through energy barriers, scattering resonances, interference between pathways, and zero-point energy in vibrational motions.

From an experimental perspective, we must consider which measurements will be most informative in testing theoretical and computational descriptions of a chemical reaction, and which will provide greatest understanding of the chemical dynamics. The experiments should be designed so that the outcomes can be directly compared with scattering calculations, but the data can also be used to construct more simple models that provide us with chemical insights about reaction mechanism and dynamics. If we choose an apparently straightforward reactive collision (one that will be the subject of further discussion in this article) involving transfer of a single atom from one reagent to another:

$$Cl + CH_4 \rightarrow HCl + CH_3 \qquad (1)$$

there are many properties that we might try to measure experimentally, as illustrated by the following incomplete list: (i) how the reaction probability depends on collision energy; (ii) what orientation of a C-H bond in CH_4 with respect to the approaching Cl favours reaction; (iii) whether kinetic energy of the reagents, or rotational or vibrational energy of the CH_4 (and energy in which of several vibrational modes) most effectively promotes reaction; (iv) whether the energy of the reaction ends up as rotation or vibration of the HCl or the CH_3 or as kinetic energy; (v) what directions the products scatter relative to the direction of approach of the reagents. We might also try to deduce the shape of the transition state for the reaction, even if it only survives for ~100 femtoseconds, and whether weak long-range interactions such as dipolar or van der Waals forces have any influence on the reaction dynamics. Measurements of any of these properties in isolation provides us with valuable insights, but we learn more if we can relate several properties in a single, correlated measurement. For example, if we can measure the angular scattering of the products with simultaneous resolution of the vibrational and rotational quantum state of the HCl and the kinetic energy of the products, we may identify some dependence of the scattering on final quantum states, and learn a great deal more than from measurements that detect all products without any quantum-state specificity.[13-16] Great strides have been made in our understanding of scattering dynamics using crossed molecular beam (CMB) methods and universal (mass-spectrometer (MS) based) detectors that can be rotated to detect the flux of products scattered into different angles. This angle-resolved flux is known as the differential cross section (DCS).[1] Correlated measurements, however, generally require a combination of molecular beam and spectroscopic detection methods (the latter to provide quantum-state specific data) and have been revolutionized by 2-D and 3-D velocity imaging techniques,[2,10,11,17] as will be illustrated in this article.

2. Principles of velocity imaging

The principles and practice for 2-D and 3-D imaging of the velocities of photofragments and the products of reactive and inelastic scattering experiments have been described in detail in recent review articles,[17,18,19] and we therefore only provide an overview here. Figure 1 illustrates the steps in the formation of a product of a reaction and its detection by velocity map imaging (VMI). At the heart of an imaging instrument are a set of carefully designed electrostatic fields which project

charged particles onto a position-sensitive detector: the positions at which the particles strike the detector depend on their velocities at the instant of their formation, whether they are electrons from a photoionization experiment, fragment atoms or radicals from photodissociation, or nascent products of a bimolecular reaction. In the case of neutral atoms, radicals or molecules, a quantum-state-specific resonance enhanced multi-photon ionization (REMPI) scheme is generally used to produce positively charged species with unchanged velocities; the recoil of a very light electron typically causes a negligible change to the velocity of the neutral species when it is ionized. The design of the electrostatic plates and lenses used to project the charged particles onto the detector is key, and modern refinements include lenses for VMI[20] (any two particles of the same mass *with the same velocity* strike the detector at the same point, regardless of whether they were formed in different locations), and weak field gradients or pulsed fields to enable slicing of an ion packet to extract only a subset of velocity components for analysis (typically only those ions with close to zero centre-of-mass (CM) frame velocity component along the imaging spectrometer axis Z).[21-23] VMI produces an image with high kinetic energy resolution, in principle enabling precise measurement of kinetic energy release distributions and thereby distinguishing channels corresponding to formation of products in different vibrational or electronic quantum states. Slice-imaging methods circumvent the need to reconstruct a full 3D velocity distribution from a 2D projection onto the imaging detector plane: although methods for the reconstruction are well-established,[10,24,25] they impose requirements of cylindrical symmetry on the experimental distribution under study and introduce noise to the final results.

Position sensitive detectors of various types are now employed in imaging experiments: a common feature is a stacked pair of microchannel plates (MCPs) which, when struck by an accelerated charged particle, generate a burst of electrons with a high gain (perhaps 10^6 electrons per incident particle). The detection of these electrons with positional information on the point of impact can be achieved by mounting a phosphor screen behind the MCP assembly; the phosphor lights up where it is excited by the electron burst, and this location can be captured by a synchronized CCD or similar video camera. Alternatively, the pulse of electrons can be recorded by using a multi-component anode behind the MCPs which is designed to give positional information, either from the time delay for the collected charge to reach two or more signal outputs (a delay-line detector) or from the fractions of the total charge collected by interleaved anode components of a specific design (e.g. wedge-and-strip detectors).[17,18] Regardless of the method used, the position sensitive

detector records two Cartesian components of the point of impact of an ion on the detector (the X and Y components) from which the X and Y velocity components can be deduced with knowledge of the point of impact for $v_X = v_Y = 0$, and the scaling factor relating radial distance on the detector to ion velocity. Accumulation of data over a large number of ion impacts on the detector builds up an image of the distribution of product velocities from a chemical reaction. It is desirable to limit the ion counts per laser shot to a small number to prevent Coulombic repulsion between the ions formed within the probe laser volume (space-charge effects, which can significantly perturb the nascent velocities). The method of determination of positions of arrival at the MCP detector can also be overwhelmed by multiple counts per laser shot. The spatial resolution of the detector can depend on a number of factors, which might include the channel size in the MCPs, the image size on the detector, the camera pixel resolution (or anode design for a delay-line or wedge-and-strip anode), the use of event counting and centring algorithms, *etc*., and more detailed discussions are provided elsewhere.[10,11,17,18,20]

3. Procedures for imaging reactive scattering

Figure 2 shows schematic diagrams of crossed molecular beam scattering instruments configured for detection of products either by a traditional detection system employing a MS, or by VMI. The two skimmed molecular beams define a plane in the laboratory, and, in the former instrument design, the MS is rotated in this plane to measure the flux of products scattered into an angle defined relative to some fixed direction in the laboratory. The times of flight of products to the detector depend on their speeds in the laboratory frame of reference, and a combined analysis of the speed and angular distributions in the lab frame can be used to reconstruct the scattering distribution in the CM frame. In this latter frame of reference, the net motion of the centre-of-mass of the collision system has been removed, and scattering angles and product velocities are referenced to the relative velocity of the colliding reagents. The chemical insights obtained from velocity-flux plots showing the CM-frame scattering angle dependence of product velocities are profound: for example, forward scattered products in the CM frame are indicative of stripping-type dynamics, with reaction occurring out to large impact parameters. The conversion of data from the lab to the CM frame is not always straightforward, however, and may involve assumptions of separability of angular scattering and product speed distributions (i.e. the kinetic energies of the

products are assumed to be independent of the angle into which they scatter). The accumulation of experimental data by measurements at a sequence of lab-frame angles is painstaking, but the rewards have been great in terms of our understanding of chemical reaction pathways: such methods continue to be powerful approaches to the study of complicated, multiple-pathway reactions of radicals of the type that occur in combustion or in planetary atmospheres (including that of Titan) and the interstellar medium.[26]

By way of contrast, the second panel of figure 2 shows an imaging detector that is fixed relative to the plane of the two molecular beams (shown as a dashed circle). The point of intersection of these beams is crossed by a laser beam which ionizes one or more reaction products – ideally with some quantum-state specificity, using a REMPI scheme, but there are also certain advantages to using a vacuum UV ionization laser, as will be discussed later. The ions formed by the laser are accelerated by electrostatic fields, separated in a time-of-fight (TOF) MS and projected onto a 2D position-sensitive detector. If the velocities of the molecular beams are well-defined, so too will be the velocity of the CM of the collision system, resulting in a net displacement of the centre of the image from zero velocity in the lab frame. A shift in the origin of the velocity map image is, however, straightforwardly corrected, giving an image of the CM-frame scattering with the advantage of multiplexed accumulation of data for all scattering angles. Care must be taken to correct for bias in the measured intensities: for example, products travelling with different velocities in the lab frame will have different projections of their velocity on the direction of propagation of the laser and thus different Doppler shifts of their resonant spectroscopic transition frequencies, but simple scanning of the laser frequency back and forth across the Doppler broadened absorption profile can compensate for this effect.

The angular scattering of the products in the CM frame is generally described by the *differential cross section* $I_R(\theta)$ (with typical units of Å^2 / sr):

$$I_R(\theta) = \frac{d\sigma_R}{d\omega} \qquad (2)$$

Here, σ_R is the integral reaction cross section and $d\omega = d\cos\theta d\phi$ is a solid angle element, expressed in terms of the CM-frame polar and azimuthal scattering angles θ and ϕ. A MS-based detection system generally measures a flux of products, whereas a laser-based ionization method will measure a density in the probe laser volume. The reaction cross section is conventionally defined

in terms of a flux[1,27] and the flux-velocity plots reported from crossed molecular beam scattering experiments are representations of the function $d^2\sigma_R/d\omega dv$, where v is the product speed in the CM frame. The conversion of velocity map images of reactive scattering distributions into this form requires a *density-to-flux* transformation which depends on the lab-frame speeds of the products. The practicalities of this procedure have been described elsewhere,[28,29] but the need for this transformation can be illustrated by an example. Reaction products that are scattered in a direction in the CM frame that means their relative velocities oppose the velocity of the CM will have lower lab-frame velocities (obtained by summing the velocity vectors of their motion in the CM frame with that of the CM) than products scattered such that their velocities are aligned with the velocity of the CM, even if the two products have the same kinetic energy and speed in the CM frame. The more slowly moving products in the lab frame will remain within the volume of the probe laser for longer than those with higher lab frame speeds, and therefore will be detected more efficiently. An experimental bias will therefore result towards detection of the slower products, but this can be corrected in the final data in a variety of ways.[10,22,30,31]

Although the schematic diagrams of crossed-molecular-beam experiments in figure 2 show the two beams intersecting at 90^o, variation of the intersection angle allows the collision energy to be altered. This strategy has been used to good effect in experiments with rotatable molecular beam sources[32-34] to study the effect of collision energy on reactive scattering dynamics; Liu, for example, has used measurements of integral and differential collision cross sections to provide definitive evidence for scattering resonances in several chemical reactions[3] – *vide infra*.

The use of skimmed molecular beams in an experiment of the type outlined in the preceding paragraphs has some down-sides however. The apparatus can be bulky, with demands for high pumping speeds to maintain appropriate vacuum conditions (although recent design innovations are reducing the experimental dimensions considerably[35]). Signal levels can also be very low because of the need for seeded and skimmed molecular beams; improvements in the design of modern pulsed valves, giving shorter pulses of higher number density are having an impact here, however.[36,37] Generation of atom or radical beams of sufficient density is also a challenge, and usually requires a discharge or photolytic source.[38,39] Two alternative strategies for VMI investigation of the dynamics of bimolecular reactions have been motivated by these difficulties with crossed-beam experiments. The two methods are illustrated in figures 3 and 4, and are referred to here as dual beam and PHOTOLOC techniques.

The dual-beam approach is based on a strategy developed by Welge and co-workers,[40] and subsequently employed by Chandler,[41] Kitsopoulos,[31] Suits[42] and others. Instead of two crossed molecular beam expansions, two parallel beams are employed, as shown in figure 3; one of the beams contains a molecular precursor to the desired atomic or radical reagent, and is intersected by a UV laser pulse which generates this reagent photolytically. Photodissociation generally imparts high speeds to the photofragments, and a well-chosen system (e.g. photolysis of Cl_2 at wavelengths of 355 nm or lower) ensures only a narrow spread of speeds, giving well-defined collision energies for subsequent collisions. Some fraction of the photofragments will fly in the direction of the second molecular beam, leading to chemical reactions, the products of which can be ionized by REMPI and their velocities captured by VMI on a detector located downstream of the photolysis and probe laser beams and oriented in a plane normal to the molecular beam directions. If the two gas expansions give molecular beams that are closely matched in speed (as will be the case for dilute gas mixtures seeded in the same bath gas such as He or Ar), the relative velocity of the collision lies close to a perpendicular line connecting the two molecular beams, and is well-defined in the image plane. The precision with which the relative velocity vector and the collision energy can be defined in the experiment is improved by the use of skimmed molecular beams. An aperture or skimmer between the two beams will further constrain the velocities of the photofragments that can successfully undergo a bimolecular reaction, but at the expense of reduction in signal levels. As demonstrated by Toomes and Kitsopoulos,[31] variation of the time delay between the laser pulses that initiate reaction and probe the products is an effective way of eliminating bias towards either forward of backward scattered products, which have different lab-frame velocities and therefore require different times to reach the volume intersected by the probe laser. Examples of the use of this method will be given in section 4.

The PHOTOLOC approach illustrated in figure 4 employs a single expansion of a gas mixture into a vacuum chamber, followed by photoinitiation of reaction and spectroscopic probing of products. This method was originally developed using laser induced fluorescence (LIF) and Doppler spectroscopy,[43] or REMPI and TOF measurements,[14,44] but VMI offers experimental advantages. The gas mixture contains a molecular reagent, and a photolytic precursor to an atomic or radical species, seeded in an inert carrier gas such as Ar. For example, for reaction (1), a mixture of CH_4 and Cl_2 is employed, with UV photolysis of Cl_2 generating the Cl atoms. In favourable cases, the two reagent gases (and the inert carrier) can be premixed, but reaction between these gases, which

may take place at the surfaces of gas lines or the pulsed nozzle, can lead to unwanted build-up of contaminants; various designs of late-mixing nozzles have therefore been implemented, in which the reagents are mixed just prior to expansion into the high vacuum chamber.[45,46] The principle underlying the PHOTOLOC method is that the distribution of scattering angles in the CM frame directly maps onto the lab-frame speed distribution of the reaction products: the relative velocity vector of the reactive collision and the velocity of the CM of the collision are close to parallel and with a common origin, so backward scattered products in the CM frame have velocity vectors that oppose the CM velocity, giving slow lab frame products, whereas the velocities of forward scattered products add to the velocity of the CM, giving fast lab-frame speeds. The relative velocity vectors for the collisions are broadly distributed in the lab frame (with a spatial distribution defined by the polarization of the photolysis laser and the velocity anisotropy parameter β for the photodissociation step that forms the atomic or radical reagent), but the analysis concentrates primarily on the speed distribution of the products, i.e. the magnitude but not the directions of the product velocities in the lab frame. Ambiguities arise in the analysis, however, if the co-product of the reaction, which is itself not probed spectroscopically, has internal degrees of freedom such as vibrational modes that can take up some of the excess energy of the reaction. The speed of the probed reaction product in the CM frame is then not single-valued, and a particular lab-frame speed can result from two or more different combinations of CM-frame speeds and scattering angles. This ambiguity can be resolved – to some extent – by incorporating into the analysis the overall spatial anisotropy of the reaction product velocities in the lab frame, which reflect the β-parameter value for the photoinitiation step, modified by the distribution of scattering angles for the bimolecular reaction. Various methods have been developed to fit the radial and angular dependences of velocity map images from PHOTOLOC experiments to incorporate lab-frame speed and velocity anisotropy information, including a procedure based on Legendre moment analysis.[47-49]

4. Examples of velocity map imaging of reactive scattering

A comprehensive review of results from VMI studies of the dynamics of bimolecular chemical reactions is beyond the scope of this article; instead, selected examples are presented that portray the power of the technique. The developments of imaging methods in chemical dynamics

concentrated on the study of photo-fragmentation of molecules,[50] but pioneering experiments on bimolecular collisions in the early 1990s established many of the methods employed in the recent studies described here. Houston and co-workers showed that CM-frame differential cross sections could be measured for the inelastic scattering of NO molecules from Ar atom using crossed molecular beam and velocity imaging of state-selectively ionized NO.[51] At about the same time, Chandler and co-workers were developing methods to image the products of bimolecular chemical reactions, initially for H + HI $\rightarrow$ H_2 + I using a single-beam expansion and UV laser photolysis of HI, with REMPI detection of H_2.[52] These first reactive experiments gave only limited information on the angular scattering of products, but modification to a dual-beam arrangement proved successful for imaging the CM-frame scattering dynamics of the H + D_2 $\rightarrow$ HD + D reaction.[41] In addition to DCS determination from the images, and for reasons that are outlined below, the measured velocities of the D atoms (tagged by REMPI and projected onto a 2D detector) should reveal structure associated with the HD formed in different vibrational and rotational energy levels. The kinetic energy resolution for early designs of imaging spectrometers was not sufficient, however, to extract quantum-state specific scattering information, and the H(D)-Rydberg atom tagging and translational spectroscopy method of Welge and co-workers[40,53] proved superior in this regard, though it lacked the multiplexing advantage for accumulation of angle-resolved data. More recently, Zare and co-workers revisited the H+D_2 reaction using PHOTOLOC and imaging methods and have derived CM-frame DCS data with high angular resolution, providing a very searching comparison with QM and QCT scattering calculations.[54]

In a generalized reaction of an atom with a diatomic molecule,

$$A + BC \rightarrow AB + C \qquad (3)$$

with reagents prepared in a molecular beam so that the internal energy of the BC molecule is close to zero, energy conservation dictates that

$$E_T - \Delta E = E'_T + E_{int}(AB) \qquad (4)$$

where E_T and E'_T are, respectively, the translational energies of reagents and products, ΔE is the energy change for the reaction, and $E_{int}(AB)$ is the internal energy of the diatomic product. The assumption has been made that the atomic product C is in its ground electronic state, so carries away no internal energy. Momentum conservation constrains the partitioning of kinetic energy

between the AB and C products. If the initial collision energy, E_T is sharply defined, the speed with which a C-atom product is travelling in the CM-frame therefore depends on the internal energy of the AB product formed in coincidence with it. Hence, a CM-frame velocity map image of the C atoms should show radial (i.e., speed-dependent) structure corresponding to C atoms of different speeds that depend on the vibrational and rotational energy levels in which the AB co-product is born. The rings of different radii in the image will have relative intensities determined by the probability of formation of the AB in these various vibrational and rotational levels. Given sufficient kinetic energy resolution, each C atom is therefore a messenger, relaying information on the energy content of its co-product AB.

For a reaction of an atom with a triatomic molecule,

$$A + BCD \rightarrow AB + CD \qquad (5)$$

there are more degrees of vibrational and rotational freedom of the two diatomic products than for the atom + diatomic molecule case, but the same principles still apply: if the CD molecule is probed by a spectroscopic technique that selects these products in a single rotational and vibrational energy level (v',J') of the ground electronic state, the internal energy, $E_{int}(CD)$, of the observed products is very precisely specified. The energy balance equation is now:

$$E_T - \Delta E = E'_T + E_{int}(AB) + E_{int}(CD) \qquad (6)$$

but the same arguments enable us to analyse the images of CD velocity distributions to derive information on the internal energies of the AB products. By changing the CD(v',J') state probed, we can unravel correlations between the internal energy states of the two products AB and CD of such a reaction: for example, a vibrationally excited level of the CD product, probed by REMPI, might be formed in coincidence with an AB product that is more likely to occupy a low vibrational level, and *vice versa*. The same reasoning applies to reactions of polyatomic molecules, with the further complexity introduced by one product (now a triatomic or larger molecule or radical) having more than one vibrational mode. This approach has been very successfully exploited by Liu and co-workers in a series of experiments studying reactions of the type

$$X + CH_4 \rightarrow HX + CH_3 \qquad (7)$$

and variants using different isotopologues of methane (CD_4, CH_2D_2, CHD_3).[55] X is one of various possible reagents, X = F, Cl, O(^{3}P) or OH, and the methyl radical product is probed by REMPI and VMI.[56-72] The REMPI spectra of CH_3 and isotopologues are sufficiently well characterized for experiments to detect radicals in specific rotational and vibrational quantum states.

The correlated motions of the products of a reaction should provide insights into the motions taking place in the transition state region of a chemical reaction, a region of the reaction pathway that is traversed in times as short as ~100 fs. In the exothermic reaction

$$F + CD_4 \rightarrow DF + CD_3 \qquad (8)$$

the methyl radical is formed vibrationally excited in its umbrella mode (ν_2), reflecting the change from a pyramidal transition state to planar structure, and there is sufficient available energy for the DF also to be formed with vibrational excitation. Velocity map images of the CD_3, probed by REMPI in vibrational levels ν_2 = 0 – 3 show rings corresponding to DF formed in vibrational levels with quantum numbers v' = 0 – 5. Each ring may exhibit a different angular shape, demonstrating product pair ($CD_3(\nu_2)$ + DF(v')) correlated differential cross sections, which evolve as the collision energy is changed in ways specific to each particular pair of products. As the data in figure 5 show, the extents of vibrational excitation in the CD_3 umbrella mode and the DF bond-stretching vibration are anti-correlated.

The reaction

$$OH + CD_4 \rightarrow HOD + CD_3 \qquad (9)$$

introduces a further degree of complexity to the idea of product pair correlations because the HOD co-product now possesses three vibrational modes. Questions can therefore be asked not just about the number of quanta of vibrational excitation in this co-product, but also about which vibrational modes are preferred, and how this preference depends on the vibrational excitation of the CD_3. Time-slice velocity map images of CD_3 (ν_2 = 0 or 2), such as those shown in figure 6, address these questions:[70,71,72] for the channel producing $CD_3(\nu_2 = 0)$, the HOD is predominantly formed with 2 quanta of O-D stretching vibration, whereas HOD with one quantum of O-D stretch is the main partner fragment for $CD_3(\nu_2 = 2)$. This anti-correlation of vibrational excitation is similar to that observed for the F + CD_4 reaction, but Liu and coworkers also observed that the O-H stretch is unexcited, indicating spectator behaviour throughout the reaction, and that the HOD bending

vibrational excitation is greater in the $CD_3(\nu_2 = 2)$ channel. The computed transition state for the reaction has a D-O bond distance of 1.32 Å that is greater than the equilibrium value of 0.97 Å in HOD, and the bend angle in the HOD moiety changes from 97^o to 103.4^o, accounting for the general trends to form HOD with vibrational excitation in the O-D stretch and bend. The correlations of these vibrational excitations with the motions of the CD_3 product may map directly from the reaction transition state, or may be influenced by the presence of a weakly bound post-transition-state complex on the PES.

Yang and coworkers recently reported development of a CMB and VMI instrument with comparable capabilities to that of Liu, but with the additional facility for dual-beam type experiments if photolytically generated reactants are required.[73,74] They demonstrated its performance with studies of the reactions of H + CD_4 and F + SiH_4, the latter with REMPI detection of SiH_3 radicals.

These CMB and VMI experiments to determine pairwise correlations are successful for a few key reasons: (i) the collision energy is very well defined using crossed or dual molecular beams; (ii) the methyl radical REMPI spectrum is sufficiently sparse in structure – in part because of the small number of vibrational modes of this tetra-atomic radical – that a laser can be tuned to ionize a single ro-vibrational quantum state; (iii) the HX co-product has widely spaced vibrational levels, the energies of which can thus be clearly resolved by observation of the KE of the methyl radical. More generally, polyatomic molecule reactions will not satisfy all these conditions: for example, larger radical products with more heavy atoms will have dense REMPI spectra, with overlapping bands from vibrational ground state and excited species. The study of these reactions will not, therefore reveal such exquisite detail as is possible for reactions such as the X + CH_4 systems; nevertheless, much can still be learned about the dynamics of the reactions of these larger molecules, as will be shown below.

The ionization potentials of many hydrocarbon and other organic radicals (denoted here as R) are sufficiently low that a vacuum UV laser (e.g. an F_2 laser at 157 nm) can be used in a one-photon ionization scheme combined with VMI detection. Suits and co-workers have exploited this strategy to good effect in studies of the scattering dynamics of a number of reactions of the type

$$X + RH \rightarrow HX + R \qquad (10)$$

with X = O(^{3}P), Cl and CN, and RH = butane or larger hydrocarbons, and selected alcohols.[75-78] These experiments have used both dual beam and, more extensively, crossed molecular beam techniques, and, in some instances of Cl-atom reactions, have been combined with 2+1 REMPI detection of the HCl co-product.[79] From the experimental images, CM-frame angular scattering and KE release data are derived, and the latter information can be used to extract distributions of internal energy of the products. One shortcoming of the method is that the VUV probe light can also photodissociate the RH molecule to produce radicals, giving a strong background signal at the velocity of the RH molecular beam that may obscure part of the velocity map image of the reactive scattering products.

The reactions of CN radicals with butane, pentane, hexane and cyclohexane to make HCN and an alkyl radical provide a recent illustration of the information that can be derived from the crossed-beam and VMI experiments with 157-nm ionization of the radical products. The scattering of the alkyl radicals is mostly backward with respect to the direction of the velocity of the alkane reagent, and energy release into translation of the products is low, typically lying in the range of 15 – 25% of the available energy. The expected early transition state for the H-atom abstraction reactions by CN radicals is indicative of much of the available energy coupling into HCN vibrational motion, consistent with the low product translational energy. A question remains, however, of why the dynamics are predominantly rebound in nature for this class of reactions with low or non-existent energy barriers.

In our own laboratory, and in our collaborative work with Kitsopoulos and colleagues, the emphasis has similarly been on studies of reactions of polyatomic molecules including hydrocarbons, hydrocarbon analogues, and various other classes of organic molecules, including alcohols, alkyl halides, ethers and cyclic ethers.[80-89] Our prior work demonstrated rich dynamics of these compounds in H-atom abstraction reactions with Cl atoms associated with the low barriers to reaction, and weakly bound complexes on the reagent and product sides of the transition state region. In addition, the low energy release and resultant slow separation of products, allows re-orientation by rotational motion to occur as the products separate and long range interactions play a part in the partitioning of the available energy into rotational degrees of freedom. In all cases, the strategy for investigation of the scattering dynamics has been to probe the HCl product with quantum-state specificity using REMPI and VMI. For experimental convenience – driven by

limitations on the amount of reactive signal observed in the experiments – the PHOTOLOC and dual-beam experimental strategies have been the methods of choice.

The reactions of Cl atoms with ethane, neopentane, tetramethyl silane (TMS), and the cyclic ethers oxirane (C_2H_4O) and oxetane (C_3H_6O) were examined using the PHOTOLOC method in our laboratory, and Brouard and coworkers have studied the reactions of Cl atoms with methane, ethane and butane.[47-49] Analysis of images using the Legendre moment (LM) method[47] generally revealed broad scattering over all angles in the CM frame, in some cases with pronounced dependence on the HCl(v=0,J) rotational level probed by REMPI, and estimates of the distributions of product translational energy were also made. The images are characterized by a product LAB frame speed distribution, P(v), and a speed-dependent anisotropy parameter, $\beta(v)$; the former is obtained from analysis of the radial dependence of the images, and the latter from the angular dependence, which varies with distance from the image centre. It is these distributions that are fitted in the LM analysis method and inverted to give CM-frame scattering data. In our experience, the numbers of radial and angular functions (Legendre polynomials in the latter case) that can be incorporated reliably in the fits is limited, and fits employing more than 3 – 5 functions in the radial and angular parts result in non-physical oscillations in the resultant distributions. This limitation is, in part, a consequence of the distribution of collision energies that accompanies a PHOTOLOC experiment, even if the experiments are carried out in the low-T environment of a supersonic expansion.[90] Care must therefore be taken to test the fitting procedure using different numbers of radial and angular polynomial functions to ensure the robustness of the outcomes.

We focus here on the results of dual beam experiments, and note that one test of the results from this method is that the derived CM-frame scattering distributions (both in scattering angle and product speed) can be used to compute the P(v) and $\beta(v)$ distributions that would be obtained from the alternative PHOTOLOC method. This computation involves inversion of the PHOTOLOC image analysis equations, and allows a direct comparison between data obtained by both experimental methods.

Figure 7 shows images obtained by Murray *et al*., for the reaction

$$Cl + CH_3OH \rightarrow HCl + CH_2OH \qquad (11)$$

using a dual-beam apparatus constructed by Kitsopoulos and coworkers.[85] The CM-frame scattering is immediately evident from the raw images, and analysis confirms that the DCS exhibits broad forward, sideways and backward scatter. Similar behaviour was observed for the reaction of Cl atoms with dimethyl ether (CH_3OCH_3). This form of the DCS is interpreted not as a signature of a deep well on the PES – electronic structure calculations do not indicate the presence of sufficiently deep wells in these Cl + RH $\rightarrow$ HCl + R abstraction reactions to support a long-lived complex – but instead is indicative of reaction over a broad range of impact parameters (*b*). This conclusion is supported by trajectory calculations which demonstrate a strong correlation between impact parameter and scattering angle in the Cl + C_2H_6 reaction;[91] small impact parameters result in rebound dynamics and backward scattering, whereas large impact parameters are associated with stripping dynamics and forward scattering. The VMI data can thus shed light on the opacity functions, P(b), for this class of reactions. The different dynamics leading to scattering into the forward and backward hemispheres also suggest that the product speed (or kinetic energy) distributions might vary with scattering angle, meaning that assumptions of separability of the speed and angular terms in the CM-frame product velocity distributions are not valid. Data from the experiments by Murray *et al*., and by Suits and coworkers for selected Cl + alkane reactions and the Cl + CH_3OH reaction do indeed illustrate changes in the KE release distributions for forward and backward scattered products. For example, for the latter reaction, the backward scattered products show greater kinetic energy release, and thus lower internal (rotational and vibrational) excitation of the CH_2OH product, than do forward scattered products. At comparable collision energies, the reactions of Cl atoms with CH_3X (X = Cl, Br) demonstrated a greater propensity for backward scattered products than the Cl + CH_3OH and Cl + CH_3OCH_3 reactions;[86] this observation was attributed to the higher barriers to reaction and tighter transition states (with potential energies that rise more rapidly as the Cl–H–C bond angle deviates from its minimum energy, near-collinear geometry), constraining collisions to occur at lower impact parameters to surmount the energy barrier for H-atom abstraction.

The dual beam experiments demonstrate that the fraction of the total available energy that is converted to product translational energy lies in the range f_T = 0.23 (for the Cl + CH_3Br reaction) to f_T = 0.42 (Cl + CH_3OCH_3), indicating in all cases that much of the available energy remains as internal excitation of the radical product; the quantum-state specific detection of HCl(v=0,J) quantifies precisely the internal energy of the HCl product, which represents only a small fraction of the total

energy. The reactions do not exhibit the approximate conservation of translational energy of reactants into products that might be expected for transfer of a light atom between two heavier species:[92] for example, for the reaction of Cl + CH_3Br at a mean reagent collision energy of 36 kJ mol^{-1}, the average kinetic energy of the products is only 11 kJ mol^{-1} despite the reaction being exothermic by -12.5 kJ mol^{-1}. The kinematic arguments for this near-conservation of translational energy thus do not appear to apply rigorously for reactions of polyatomic molecules, in which one product can absorb energy into its rotational and many vibrational degrees of freedom.

More recent results from a dual beam and VMI experiment in our laboratory illustrate a potential problem with the experimental technique. Data were obtained for the reaction of Cl + C_2H_6, using photolysis of Cl_2 at a wavelength of 355 nm in one molecular beam, and reaction with ethane molecules in a skimmed molecular beam located 17-mm above.[93] The dual beam data were contrasted with CMB and VMI data for the same reaction from Suits and coworkers;[79] both experiments employed (2+1) REMPI detection of the HCl(v=0,J) products. Although the DCS data agree in the forward scattered direction, the dual-beam experiments appear to undercount the backward scattered products. These backward scattered products move more slowly in the LAB frame than do the forward scattered products, because for backward scatter the CM-frame velocities oppose the centre-of-mass velocity vector. The experiments are therefore conducted over a range of time delays between the photolysis and probe laser pulses to minimize any bias against slower or faster moving products (essentially using an experimental method to correct for density to flux conversion effects). Extensive Monte Carlo simulations of the experimental method, which incorporate parameters describing the molecular beam expansions, laser pulses and locations, reaction energetics, CM-frame scattering, *etc*., show no clear-cut reason for the bias. By process of elimination, it is therefore attributed to secondary collisions of the products with the skimmed molecular beam of RH molecules; the slower-moving backward scattered products spend longer within the volume swept out by this molecular beam before REMPI detection than do the forward scattered products, and are thus more prone to further collisions that might scatter them away from the probe laser region. Possible remedies to this problem include use of more dilute molecular beams, seeded in He carrier gas to reduce collision cross sections, lower backing pressures behind the nozzle orifices, and smaller diameter skimmer apertures.

Two approaches have been developed to correct the recent dual beam data for this under-detection of products scattered into the backward direction. A pragmatic strategy is to calibrate

the under-detection by comparing dual beam data for the Cl + ethane reaction with CMB and VMI data from Suits and coworkers, and to use the resultant scattering-angle dependent calibration function to correct images for other reactions. The validity of this method can be tested by use of the corrected DCSs to simulate single-beam PHOTOLOC data, as was discussed above. An alternative approach is to model the depletion of backward scattered products within the Monte Carlo simulation of the experiment, using a depletion factor that depends on the computed time spent within the zone of the RH molecular beam;[93] this time depends on the LAB frame speed, and thus on the CM-frame scattering angle.

5. Quantum mechanical effects in chemical reactions

Many features of a chemical reaction can be understood in terms of models based on description of collisions by classical equations of motion, with impact parameters and line-of-centre collision energies influencing the CM-frame scattering angle distributions. Quasi-classical trajectory (QCT) methods, in which trajectories are propagated on a PES using Newtonian (or Hamiltonian) mechanics, successfully capture many of the dynamical features of a host of chemical reactions: even for the H + D_2 reaction, with light atoms for which QM effects might be expected to be most pronounced, most experimental data can be reproduced with QCT calculations on a state-of-the-art PES.[94] In the case of reactions of polyatomic molecules, generation of a multi-dimensional PES of sufficient accuracy for the outcomes of trajectory propagation to be compared meaningfully with experiments is a considerable challenge, and the QCT calculations will not constrain the vibrational energy content in the many degrees of freedom to remain at or above the zero-point energy level. Both these problems can be addressed, however, allowing comparison of QCT calculations with experimental data for reactions such as Cl + $C_2H_6 \rightarrow$ HCl + C_2H_5. In this particular case, our calculations used a semi-empirical Hamiltonian to generate PE points "on-the-fly" at molecular configurations sampled by individual trajectories, and were thus able to propagate trajectories from reagents through to products without computation of a global PES.[91,95] Figure 8 shows comparisons of measured and calculated angular scattering distributions: from examination of the QCT calculations, we demonstrated a clear correlation between impact parameter and scattering angle, with abstraction reactions at large values of *b* leading to forward scattering. Note also that the QCT outcomes could, in principle, be used to simulate the experimental velocity-map image.

Some features of chemical reactions are inherently quantum mechanical in nature, however, and will not be well accounted for in QCT simulations. Such features include tunnelling through PE or centrifugal barriers, scattering resonances,[3] and non-adiabatic dynamics.[96-99] The VMI of reactive scattering, with measurement of integral and differential cross sections as a function of collision energy, has been pivotal in identifying signatures of reactive scattering resonances.

Detailed discussions of types of scattering resonance can be found in, for example, the recent review of bimolecular scattering dynamics by Yang.[3] A scattering resonance is qualitatively described as a short-lived, metastable species that is quasi-bound along the reaction coordinate, despite the possible presence of a barrier to reaction and the absence of any deep potential wells. The circumstances giving rise to a Feshbach resonance are illustrated schematically in figure 9 for a PES with no wells in the zero-point vibrational adiabat: the vibrationally adiabatic potentials for the ground electronic state are depicted, and the reacting molecules can become trapped in the energy wells on these adiabats because they lie lower in energy than the associated asymptotes corresponding to vibrationally excited products. The resonances can decay by vibrationally non-adiabatic coupling to lower energy vibrational adiabats, giving the resonance states short lifetimes. A challenge for experimentalists has been to identify asymptotic properties of a reaction that can be attributed to this Feshbach resonance behaviour. Theoretical calculations of reactive scattering in triatomic systems have played an important role in guiding the interpretation of various forms of experimental data to provide definitive evidence of scattering resonances. For example, scattering calculations show that the resonances have energy dependence, and are therefore best observed in experiments that span a range of collision energies.

Liu and coworkers[100-103] have reported steps that occur in the integral cross section as E_{coll} increases, that they attribute to resonances; the steps have broad widths that are a consequence of overlapping resonance features which shift in energy for different orbital angular momentum of the collision (and thus, in a classical picture, different impact parameters). Plots of the energy dependent differential cross sections for reactions such as those of F + HD and Cl + CH_4 show two distinct features that are more revealing:[101,104] the first is a ridge that starts as backward scattering at low collision energies, but evolves to more sideways and forward scattering as the collision energy increases; the second is sharp scattering into both the forward and backward hemispheres that occurs over a limited energy range. The former feature is attributed to direct reactive scattering, which can occur at increasing impact parameters as the collision energy is raised. The

second feature is argued to be a signature of resonances, and may only be evident in particular product pair channels (such as the HCl(v=1) + CH_3(v=0) pathway for the Cl + CH_4 reaction). The cause of the resonance in this reaction is different from those in the F-atom reactions (as shown in fig 9), and is illustrated in figure 10. The vibrationally adiabatic state connecting Cl + CH_4(v_1=1) and HCl(v=1) + CH_3(v=0) drops in energy in the region of the barrier on the electronic PES because of a decrease in the symmetric stretch vibrational frequency in this region. The resultant well in the vibrationally adiabatic potential may support a quasi-bound vibrational mode, assigned as having one quantum of CH_3 symmetric stretch and zero quanta of excitation of all other modes. Collisions of Cl atoms with vibrationally ground state CH_4 with sufficient collision energy can couple into this quasi-bound state by translational-to-vibrational energy transfer (with low probability). The state survives sufficiently long for rotation of the complex before energy in other degrees of freedom couples into the reaction coordinate and causes the resonance to decay, either to CH_3(v=0) + HCl(v=1) or CH_3(v=0) + HCl(v=0) products.

Further signatures of resonances are also observed, such as anomalous rotational excitation of the products, or very specific product vibrational pair correlations. For example, velocity map images reveal the near-threshold formation of symmetric stretch excited CH_3(v_1=1) with HF(v=2) in the reaction of F atoms with CH_4, indicating a specific dissociation pathway for the resonance, which is assigned to an F-H-CH_3 complex with 3 quanta of excitation in the intermolecular F – H bond, by coupling to the symmetric stretch motion of the CH_3 moiety.[102] The observation of onset of forward-backward peaking in the DCS at specific energies, however, appears to be the most clear-cut signature so far identified in experiments, and is most effectively resolved using VMI techniques.

The preceding discussion about resonances illustrated the subtle roles of vibrationally adiabatic and non-adiabatic effects on the scattering dynamics. The dynamics of chemical reactions are generally assumed to occur on a single *electronic* PES, in accord with the Born-Oppenheimer approximation, and are therefore described as being electronically adiabatic. Couplings between PESs, induced, for example by terms neglected in the Born-Oppenheimer approximation such as those arising from the kinetic energy of the atoms, can, however, induce reactive flux to undergo electronically non-adiabatic transitions from one PES to another. Such dynamics are exemplified by the reverse of reaction (1)

$$CH_3 + HCl \rightarrow CH_4 + Cl(^2P_J) \quad (12)$$

in which the PES correlates adiabatically only to Cl atoms in their ground spin-orbit state, $Cl(^2P_{3/2})$. Production of spin-orbit excited $Cl^*(^2P_{1/2})$ atoms requires a non-adiabatic transition to a higher-lying PES, and REMPI detection of Cl atoms demonstrated a branching ratio of 15% for the Cl* products at a mean collision energy of the reagents of 93.3 kJ mol^{-1}.[96] The PHOTOLOC method was employed by Retail *et al*. in combination with VMI of both Cl and Cl* atoms to demonstrate indistinguishable scattering dynamics for the two channels of reaction (12), from which it was deduced that the non-adiabatic couplings between PESs occur on the products' side of the barrier to reaction.[97,98] Work is in progress in our laboratory to study the effects of collision energy on the non-adiabatic transition probabilities, using dual-beam and VMI methods.[93]

6. Ion-molecule reactions

The discussion so far has concentrated on reactions of neutral species (atoms, molecules and radicals), for which one of the products must be ionized by REMPI or one-photon VUV absorption prior to accumulation of a velocity image. Reactions of atomic or molecular *ions* with neutral species will however, produce a charged reaction product that can be projected onto a position sensitive detector by electrostatic fields without need for a laser excitation step. Guided ion beam and energy-selection methods can also be employed to prepare the reagents with well-defined collision energies, and to vary the collision energy to map out reaction excitation functions. Price and co-workers have, for example, used a delay-line position-sensitive detector to derive CM-frame scattering distributions for a number of reactions of doubly charged cations (dications) such as CO_2^{2+}, CF_2^{2+} and N_2^{2+}, which exhibit bond-forming, dissociative and electron-transfer pathways.[105] If two mono-cations are formed from a reactive collision, both can be detected in coincidence and their velocities measured; in the case of pathways forming three products, deductions can then be made about the velocities of the neutral third product by momentum conservation arguments.

The study by Wester and coworkers[106] of a classic S_N2 reaction mechanism:

$$Cl^- + CH_3I \rightarrow ClCH_3 + I^-$$

under single-collision conditions in the gas phase provides an elegant example of how the intrinsic reaction dynamics can be separated from any solvent effects that will influence the mechanism under the more common solution-phase conditions. Ion-dipole interactions between Cl^- and CH_3I reagents, and between CH_3Cl and I^- products give rise to PE wells either side of a transition state barrier that is computed to lie lower in energy than the separated reagents. An evolution is observed from isotropic scattering at a collision energy of 38 kJ mol^{-1} to forward scattering of the I^- with respect to the Cl^- velocity for collision energies of 73 kJ mol^{-1} and above. This latter scattering is consistent with direct nucleophilic substitution and a Walden inversion. At the highest studied collision energy of 183 kJ mol^{-1}, a further indirect mechanism was identified that gives forward-backward scattering as a minor channel. With the aid of trajectory calculations, this pathway was attributed to a "roundabout" mechanism in which the Cl^- collides with the methyl group, inducing rotation of the CH_3I. The CH_3I undergoes a full rotation, taking ~500 – 600 fs, before the Cl^- successfully displaces an I^- anion.

7. Conclusions

This perspective article has illustrated the power of VMI methods for the detailed study of the dynamics of reactive collisions of isolated, gas-phase atoms, radicals, molecules or ions. The level of information extracted from these experiments is unprecedented for bimolecular reactions, and provides profound tests of theoretical and computational studies of chemical mechanisms. As VMI methods develop further, employing detectors that resolve 3D velocity information, and crossed molecular beam machines reduce in size and complexity – an advantage of a fixed detector that collects products from all scattering angles simultaneously – the scope for many further such studies will be greatly increased. The discussion in this article has focussed on single pathways for a chemical reaction, leading to a particular set of products, but many reactions exhibit branching to multiple, chemically distinct product channels. Such competition between reaction pathways is most evident for radical species, many of which have been studied by traditional CMB and MS methods. If VMI methods can be coupled with laser detection of multiple products and mass-resolution without loss of the multiplexing advantages that are characteristic of the technique, there is great potential for further investigation of these multi-channel reactions. Multi-mass imaging methods, in which images are accumulated for products of different masses

simultaneously, are currently in development, using a range of strategies, and may provide the necessary experimental capabilities.[107-110]

Although 3D VMI is now well-established, and has been used to very good effect in studies of bimolecular reactions, the additional dimension of time remains to be exploited effectively. VMI with ultrafast (fs – ps) time resolution has proven to be a powerful combination for the study of molecular photodissociation and photoionization mechanisms,[111,112] but is more challenging to implement for bimolecular collisions because of the ill-defined – and very long compared to the ultrafast timescale – interval between creation of reagents and collisions that lead to products. Constraining reactions to occur within clusters produced by supersonic expansions through pulsed nozzles is a strategy that has been employed for bimolecular reactions,[113-117] but that has yet to be coupled with VMI and ultrafast laser methods for optimum experimental information. Such cluster studies also have the potential to provide a bridge between gas and condensed-phase reaction mechanisms. The comparison of dynamics in the gas and condensed phases can, in principle, be used to deduce the effect of a solvent on the features of a reactive PES such as barrier heights and locations, and the couplings between PESs, but experimental studies of the dynamics of bimolecular reactions in liquid solution are sparse. As VMI methods extend to gas phase studies of polyatomic molecules, and ultrafast time-resolved infra-red spectroscopy methods explore further the dynamics of reactions in solution,[118-124] direct comparisons between the same reactive systems in the absence and presence of solvent should deliver increasingly valuable insights leading to quantitative understanding of the role of solvation on reaction mechanisms.

Acknowledgements

The authors gratefully acknowledge EPSRC for financial support through the Programme Grant EP/G00224X and the University of Bristol for a postgraduate scholarship (R.A.R.). S.J.G. thanks the Leverhulme Trust for an Early Career Research Fellowship and A.J.O.E. thanks the Royal Society and the Wolfson Foundation for a Research Merit Award.

Figure captions

Figure 1: Schematic diagram of the study of the dynamics of a bimolecular reaction using a velocity map imaging spectrometer. The enlarged region shows (i) collision of two reagents; (ii) recoil of the products, one of which has a velocity $\underline{v}$; (iii) ionization of one product by the probe laser (resonance-enhanced if quantum-state specific information is required). The resultant cations are extracted by electric fields from the repeller and extractor plates and focused by the extractor and lens assembly onto the position sensitive detector. The point of impact is recorded by, for example, a camera or a delay-line anode. The position of the impact relative to the image centre is proportional to the initial velocity vector $\underline{v}$, with proportionality factor α determined from a calibration experiment.

Figure 2: A comparison of detection methods for crossed molecular beam studies of bimolecular reaction dynamics. The left-hand panel shows two intersecting beams from skimmed nozzle sources, and a mass spectrometer (MS) that is rotated inside the vacuum chamber to measure the flux of products, $I(\Theta)$ scattered at different laboratory angles Θ. The measurements include times of flight of products, which are determined at each scattering angle, and thus each position of the detector. The right-hand panel shows the how laser ionization and velocity map imaging can be used to observe scattering into all laboratory frame angles at the same time. Accumulation of events over a large number of probe laser pulses generates a velocity image of the type shown in the inset, analysis of which gives speed and scattering angle distributions in the centre-of-mass frame.

Figure 3: Illustration of a dual-beam and velocity map imaging experiment to study bimolecular reaction dynamics. The sequence of steps shown is: (i) and (ii) separate, parallel molecular beam expansions are made of the two reagents (in this case illustrated as Cl_2 and ethane in argon carrier gas); (iii) photolysis of the molecules in the lower molecular beam (in this case $Cl_2 \rightarrow Cl + Cl$) generates translationally hot atoms or radicals, some of which fly upwards and intersect the upper beam where (iv) reaction takes place (here, $Cl + C_2H_6 \rightarrow HCl + C_2H_5$), as shown in the magnified view; (v) products (HCl) that scatter into the focal region of the probe laser can be ionized, and (vi) are extracted by VMI fields to the position sensitive detector.

Figure 4: Illustration of the PHOTOLOC strategy combined with velocity map imaging to study reactive scattering. In the PHOTOLOC experiments,the sequence of events is: (i) expansion of a mixture of reagents through a nozzle into a vacuum chamber to form a molecular beam; (ii) the molecular beam is crossed by two overlapped and counter-propagating lasers, the first of which photodissociates one species to initiate reaction, and the second laser ionizes one reaction product; (iii) the ionized products are extracted to a position sensitive detector with electric fields designed for velocity map imaging; (iv) the point of impact on the detector is recorded.

Figure 5: Correlated populations of $CD_3(0,v_2,0,0)$ and DF(v) vibrationally state specific products of the reaction of F atoms with CD_4 at a collision energy of 35 kJ mol^{-1}. The data are taken from ref. 63 and were derived from a crossed molecular beam and velocity map imaging experiment.

Figure 6: Velocity map images obtained by REMPI detection of the CD_3 radical products of the reaction OH + $CD_4 \rightarrow$ HOD + CD_3: (a) detection of CD_3(v=0) at a collision energy E_{coll} = 41.8 kJ mol^{-1}; (b) detection of $CD_3(v_2=2)$ with E_{coll} = 44.3 kJ mol^{-1}. Orange lines show the Newton diagram for the collision and rings indicate the maximum recoil speeds of CD_3 radicals formed in coincidence with HOD molecules with the indicated number of vibrational quanta in the O-D stretch, bend and O-H stretching modes. The figure is reproduced with permission from ref. 70.

Figure 7: Velocity map images for (a) HCl(v=0,J=2) and (b) HCl(v=0, J=5) products of the reaction of Cl atoms with methanol. The images were obtained using a dual-beam method, with a mean collision energy of 23 kJ mol^{-1}. Forward scattering with respect to the velocities of the Cl atom reagents (0^o) corresponds to the top of each image. The scattering distributions are subtly dependent on the rotational level of the HCl.

Figure 8: Comparison of the angular scattering distributions for HCl from the reaction of Cl atoms with C_2H_6 obtained by velocity map imaging (solid line – from ref. 79) and quasi-classical trajectory calculations (circles).

Figure 9: A schematic illustration of a Feshbach resonance in a chemical reaction. The diagram portrays energies along the pathway for a generic reaction A + BC $\rightarrow$ AB(v') + C. The solid lines show vibrationally adiabatic potential energy curves, with the AB product formed in vibrational

level v' = 0 – 3. The dashed arrow denotes the collision energy E_{coll} of the reagents, and the horizontal dashed lines are vibrational states trapped within shallow potential wells on the products' side of the reaction barrier. These wells can arise from van der Waals type interactions, or, as in the case of the v' = 3 adiabat, from a reduction in the A-B vibrational frequency when C is in close proximity. The collision energy is not sufficient to surmount the activation barrier, but reaction can occur by a tunnelling mechanism. At the energies of the resonances shown for the v'=3 adiabat, products can be temporarily trapped in the vibrationally adiabatic potential well, but with insufficient energy to dissociate to the AB(v'=3) + C asymptote, so instead decay to AB(v'=2) products. The diagram is modelled on the $F + H_2 \rightarrow HF + H$ reaction.

Figure 10: Schematic diagram of the variation of the energies of selected vibrationally adiabatic potential energy curves with reaction coordinate for the $Cl + CH_4 \rightarrow HCl + CH_3$ reaction. The transition state on the lowest adiabat is denoted by $[Cl\text{-}H\text{-}CH_3]^{\#}$. The potential energy well in the adiabat for reaction of symmetric stretch excited $CH_4(v_1=1)$ with Cl atoms supports a postulated resonance state indicated by a dashed line.[104]

References

[1] R.D. Levine, *Molecular Reaction Dynamics*, Cambridge University Press, Cambridge, 2005.
[2] M. Brouard and C. Vallance, *Tutorials in Molecular Reaction Dynamics*, Royal Society of Chemistry (2010).
[3] X. Yang, *Annu. Rev. Phys. Chem.*, 2007, **58**, 433.
[4] A.I. Boothroyd, W.J. Keogh, P.G. Martin and M.R. Peterson, *J. Chem. Phys.*, 1996, **104**, 7139.
[5] G.L. Li, H.J. Werner, F. Lique and M.H. Alexander, *J. Chem. Phys.*, 2007, **127**, 174302.
[6] D.H. Zhang, M.A. Collins and S.-Y. Lee, *Science*, 2000, **290**, 961.
[7] A. Gonzalez-Lafont, T.N. Truong and D.G. Truhlar, *J. Phys. Chem.*, 1991, **95**, 4618.
[8] S.T. Banks, C.S. Tautermann, S.M. Remmert and D.C. Clary, *J. Chem. Phys.*, 2009, **131**, 044111.
[9] S. Rudić, C. Murray, J.N. Harvey and A.J. Orr-Ewing, *J. Chem. Phys*. 2004, **120**, 186.
[10] *Imaging in Chemical Dynamics*, Ed. A.G. Suits and R.E. Continetti, ACS Books, Washington DC, 2000.
[11] *Imaging in Molecular Dynamics, Technology and Applications*, ed. B.J. Whitaker, Cambridge University Press, Cambridge, 2003.
[12] S.C. Althorpe and D.C. Clary, *Annu. Rev. Phys. Chem*., 2003, **54**, 493.
[13] C. Murray and A.J. Orr-Ewing, *Int. Rev. Phys. Chem.*, 2004, **23**, 435.
[14] W.R. Simpson, A.J. Orr-Ewing, and R.N. Zare, *Chem. Phys. Lett*., 1993, **212**, 163.
[15] W.R. Simpson, T.P. Rakitzis, S.A. Kandel, A.J. Orr-Ewing, and R.N. Zare, *J. Chem. Phys.*, 1995, **103**, 7313.
[16] A.J. Orr-Ewing, W.R. Simpson, T.P. Rakitzis, S.A. Kandel, and R.N. Zare, *J. Chem. Phys*., 1997, **106**, 5961.
[17] M.N.R. Ashfold, N.H. Nahler, A.J. Orr-Ewing, O.P.J. Vieuxmaire, R.L. Toomes, T.N. Kitsopoulos, I.A. Garcia, D.A. Chestakov, S.M. Wu and D.H. Parker, *Phys. Chem. Chem. Phys*., 2006, **8**, 26.
[18] A.I. Chichinin, K.-H. Gericke, S. Kauczok and C. Maul, *Int. Rev. Phys. Chem*., 2009, **28**, 607.
[19] C. Vallance, Phil. Trans. Roy. Soc. A, 2004, **362**, 2591.
[20] A.T.J.B. Eppink and D.H. Parker, *Rev. Sci. Instrumen.*, 1997, **68**, 3477.
[21] D. Townsend, M.P. Minitti and A.G. Suits, *Rev. Sci. Instrumen.*, 2003, **74**, 2530.
[22] J.J. Lin, J. Zhou, W. Shiu and K. Liu, *Rev. Sci. Instrumen.*, 2003, **74**, 2495.
[23] C.R. Gebhardt, T.P. Rakitzis, P.C. Samartzis, V. Ladopoulos and T.N. Kitsopoulos, *Rev. Sci. Instrumen.*, 2001, **72**, 3848.
[24] V. Dribinski, A. Ossadtchi, V.A. Mandelshtam and H. Reisler, *Rev. Sci. Instrumen.*, 2002, **73**, 2634.
[25] G.M. Roberts, J.L. Nixon, J. Lecointre, E. Wrede and J.R.R. Verlet, *Rev. Sci. Instrumen.*, 2009, **80**, 053104.
[26] P. Casavecchia, F. Leonori, N. Balucani, R. Petrucci, G. Capozza, and E. Segoloni, *Phys. Chem. Chem. Phys.*, 2009, **11**, 46.
[27] P.J. Dagdigian, Chapter 23 in *Atomic and Molecular Beam Methods,* Volume 1, ed. G. Scoles, Oxford University Press (1988)
[28] D.M. Sonnenfroh and K. Liu, *Chem. Phys. Lett*. 1991, **176**, 182.
[29] Y.-T. Hsu, K. Liu, L.A. Pederson and G.C. Schatz, *J. Chem. Phys.*, 1999, **111**, 7921.
[30] K.T. Lorenz, D.W. Chandler and G.C. McBane, *J. Phys. Chem. A*, 2002, **106**, 1144.
[31] R.L. Toomes and T.N. Kitsopoulos, *Phys. Chem. Chem. Phys.*, 2003, **5**, 2481.
[32] G. Hall, K. Liu, M.J. McAuliffe, C.F. Giese and W.R. Gentry, *J. Chem. Phys.*, 1984, **81**, 5577.
[33] C. Naulin and M. Costes, *Chem. Phys. Lett.*, 1999, **310**, 231.
[34] R.G. MacDonald and K. Liu, *J. Chem. Phys.*, 1989, **91**, 821.
[35] P. Jansen, D.W. Chandler and K.E. Strecker, *Rev. Sci. Instrumen.*, 2009, **80**, 083105.
[36] U. Even, J. Jortner, D. Noy, N. Lavie and C. Cossart-Magos, *J. Chem. Phys.*, 2000, **112**, 8068.
[37] D. Irimia, R. Kortekaas and M.H.M. Janssen, *Phys. Chem. Chem. Phys.*, 2009, **11**, 3958.
[38] M.C. van Beek and J.J. ter Meulen, *Chem. Phys. Lett.*, 2001, **337**, 237.
[39] R.A. Rose, A.J. Orr-Ewing, C.-H. Yang, K. Vidma, G.C. Groenenboom, and D.H. Parker, *J. Chem. Phys.*, 2009, **130**, 034307.
[40] L. Schnieder, K. Seekamp-Rahn, F. Liedeker, H. Steuwe and K.H. Welge, *Faraday Discuss. Chem. Soc.*, 1991, **91**, 259
[41] T.N. Kitsopoulos, M.A. Buntine, D.P. Baldwin, R.N. Zare and D.W. Chandler, *Science*, 1993*,* **260**, 1605.
[42] X. Liu, R.L. Gross and A.G. Suits, *J. Chem. Phys.*, 2002, **116**, 5341.
[43] M. Brouard, S.P. Duxon, P.A. Enriquez, R. Sayos and J.P. Simons, *J. Phys. Chem.*, 1991, **95**, 8169.
[44] N.E. Shafer, A.J. Orr-Ewing, W.R. Simpson, H. Xu, and R.N. Zare, *Chem. Phys. Lett*., 1993, **212**, 155
[45] S. Rudić, D. Ascenzi and A.J. Orr-Ewing, *Chem. Phys. Lett.*, 2000, **332**, 487.
[46] J.P. Camden, H.A. Bechtel and R.N. Zare, *Rev. Sci. Instrumen.*, 2004, **75**, 556.
[47] M.J. Bass, M. Brouard, C. Vallance, T.N. Kitsopoulos, P.C. Samartzis, and R.L. Toomes, *J. Chem. Phys.,* 2003, **119**, 7168.

[48] M.J. Bass, M. Brouard, C. Vallance, T.N. Kitsopoulos, P.C. Samartzis and R.L. Toomes, *J. Chem. Phys.*, 2004, **121**, 7175.
[49] M.J. Bass, M. Brouard, R. Cireasa, A.P. Clark and C. Vallance, *J. Chem. Phys.*, 2005, **123**, 094301.
[50] D.W. Chandler and P.L. Houston, *J. Chem. Phys.*, 1987, **87**, 1445.
[51] A.G. Suits, L.S. Bontuyan, P.L. Houston and B.J. Whitaker, *J. Chem. Phys.*, 1992, **96**, 8618
[52] M.A. Buntine, D.P. Baldwin, R.N. Zare and D.W. Chandler, *J. Chem. Phys.*, 1991, **94**, 4672.
[53] L. Schnieder, W. Meier, K.H. Welge, M.N.R. Ashfold and C.M. Western, *J. Chem. Phys.*, 1992, **97**, 3157.
[54] N.T. Goldberg, J. Zhang, D.J. Miller and R.N. Zare, *J. Phys. Chem. A*, 2008, **39**, 9267.
[55] K. Liu, *Phys. Chem. Chem. Phys.*, 2007, **9**, 17.
[56] J. Zhou, J.J. Lin, W. Shiu, S.-C. Pu and K. Liu, *J. Chem. Phys.*, 2003, **119**, 2538.
[57] J.J. Lin, J. Zhou, W. Shiu and K. Liu, *Science*, 2003, **300**, 966.
[58] J. Zhou, J.J. Lin, W. Shiu and K. Liu, *J. Chem. Phys.*, 2003, **119**, 4997.
[59] J. Zhou, J.J. Lin and K. Liu, *J. Chem. Phys.*, 2003**, 119**, 8289.
[60] W. Shiu, J.J. Lin and K. Liu, *J. Chem. Phys.*, 2004, **120**, 117.
[61] J. Zhou, W. Shiu, J.J. Lin and K. Liu, *J. Chem. Phys.*, 2004, **120**, 5863
[62] J. Zhou, W. Shiu, J.J. Lin and K. Liu, *J. Chem. Phys.*, 2006, **124**, 104309.
[63] J. Zhou, J.J. Lin, W. Shiu and K. Liu, *Phys. Chem. Chem. Phys.*, 2006, **8**, 3000.
[64] B. Zhang, S. Yan and K. Liu, *J. Phys. Chem. A*, 2007, **111**, 9263.
[65] W. Zhang, H. Kawamata and K. Liu, *Science*, 2009, **325**, 303.
[66] J. Zhou, J.J. Lin, B. Zhang and K. Liu, *J. Phys. Chem. A*, 2004, **108**, 7832.
[67] J. Zhou, B. Zhang, J.J. Lin and K. Liu, *Mol. Phys.*, 2005, **103**, 1757.
[68] H. Kawamata, S. Tauro and K. Liu, *Phys. Chem. Chem. Phys.*, 2008, **10**, 4378.
[69] Y.-T. Wu and K. Liu, *J. Chem. Phys.*, 2008, **129**, 154302.
[70] B. Zhang, W. Shiu, J.J. Lin and K. Liu, *J. Chem. Phys.*, 2005, **122**, 131102.
[71] B. Zhang, W. Shiu and K. Liu, *J. Phys. Chem. A*, 2005, **109**, 8983.
[72] B. Zhang, W. Shiu and K. Liu, *J. Phys. Chem. A*, 2005, **109**, 8989.
[73] G. Wu, W. Zhang, H. Pan, Q. Shuai, B. Jiang, D. Dai and X. Yang, *Rev. Sci. Instrumen.,* 2008, **79**, 094104.
[74] W. Zhang, G. Wu, H. Pan, Q. Shuai, B. Jiang, D. Dai and X. Yang, *J. Phys. Chem. A*, 2009, **113**, 4652.
[75] M. Ahmed, D.S. Peterka and A.G. Suits, *Chem. Phys. Lett.*, 2000, **317**, 264.
[76] M. Ahmed, D.S. Peterka and A.G. Suits, *Phys. Chem. Chem. Phys.*, 2000, **2**, 861.
[77] C. Huang, W. Li, A.D. Estillore and A.G. Suits, *J. Chem. Phys.*, 2008, **129**, 074301.
[78] X. Liu, R.L. Gross, G.E. Hall, J.T. Muckerman, and A.G. Suits, *J. Chem. Phys.*, 2002, **117**, 7947.
[79] C. Huang, W. Li and A.G. Suits, *J. Chem. Phys.*, 2006, **125**, 133107.
[80] C. Murray, J.K. Pearce, S. Rudić, B. Retail, and A.J. Orr-Ewing, *J. Phys. Chem. A*, 2005, **109**, 11093.
[81] S. Rudić, C. Murray, D. Ascenzi, H. Anderson, J.N. Harvey and A.J. Orr-Ewing, *J. Chem. Phys*., 2002, **117**, 5692.
[82] S. Rudić, C. Murray, J.N. Harvey and A.J. Orr-Ewing, *Phys. Chem. Chem. Phys*., 2003, **5**, 1205.
[83] C. Murray, B. Retail and A.J. Orr-Ewing, *Chem. Phys*., 2004, **301**, 239.
[84] J.K. Pearce, C. Murray, P.N. Stevens and A.J. Orr-Ewing, *Mol. Phys.*, 2005, **103**, 1785.
[85] C. Murray, A.J. Orr-Ewing, R.L. Toomes and T.N. Kitsopoulos, *J. Chem. Phys.*, 2004, **120**, 2230.
[86] R.L. Toomes, A.J. van den Brom, T.N. Kitsopoulos, C. Murray and A.J. Orr-Ewing, *J. Phys. Chem. A*, 2004, **108**, 7909.
[87] J.K. Pearce, C. Murray and A.J. Orr-Ewing, *Phys. Scrip*., 2006, **73**, C14 – 19.
[88] J.K. Pearce, S.J. Greaves, B. Retail, R.A. Rose and A.J. Orr-Ewing, *J. Phys. Chem. A,* 2007, **111**, 13296.
[89] B. Retail, R.A. Rose, J.K. Pearce, S.J. Greaves and A.J. Orr-Ewing, *Phys. Chem. Chem. Phys*. 2008, **10**, 1675.
[90] W.J. van der Zande, R. Zhang, R.N. Zare, K.G. McKendrick and J.J. Valentini, *J. Phys. Chem*. 1991, **95**, 8205.
[91] S.J. Greaves, A.J. Orr-Ewing and D. Troya, *J. Phys. Chem. A,* 2008, **112**, 9387.
[92] C.A. Piconatto, A. Srivastava and J.J. Valentini, *J. Chem. Phys.,* 2001, **114**, 1663.
[93] R.A. Rose, S.J. Greaves and A.J. Orr-Ewing, *Mol. Phys*., in press.
[94] S.J. Greaves, E. Wrede, N.T. Goldberg, J. Zhang, D.J. Miller and R.N. Zare, *Nature*, 2008, **454**, 88.
[95] S.J. Greaves, J. Kim, A.J. Orr-Ewing and D. Troya, *Chem. Phys. Lett*., 2007, **441**, 171.
[96] B. Retail, J.K. Pearce, C. Murray and A.J. Orr-Ewing, *J. Chem. Phys*., 2005, **122**, 101101.
[97] B. Retail, S.J. Greaves, J.K. Pearce, R.A. Rose and A.J. Orr-Ewing, *Phys. Chem. Chem. Phys.*, 2007, **9**, 3261.
[98] B. Retail, J.K. Pearce, S.J. Greaves, R.A. Rose and A.J. Orr-Ewing, *J. Chem. Phys*., 2008, **128**, 184303.
[99] B.F. Parsons and D.W. Chandler, *J. Chem. Phys.*, 2005, **122**, 174306.
[100] R.T. Skodje, D. Skouteris, D.E. Manolopoulos, S.H. Lee, F. Dong, and K. Liu, *J. Chem. Phys.*, 2000, **112**, 4536.

[101] R.T. Skodje, D. Skouteris, D.E. Manolopoulos, S.H. Lee, F. Dong, and K. Liu, *Phys. Rev. Lett.*, 2000, **85**, 1206.
[102] W. Shiu, J.J. Lin and K. Liu, *Phys. Rev. Lett.*, 2004, **92**, 103201.
[103] J. Zhou, J.J. Lin and K. Liu, *J. Chem. Phys.*, 2004, **121**, 813.
[104] B. Zhang and K. Liu, *J. Chem. Phys.*, 2005, **122**, 101102.
[105] S.D. Price, *Int. J. Mass Spec.*, 2007, **260**, 1.
[106] J. Mikosch, S. Trippel, C. Eichhorn, R. Otto, U. Lourderaj, J.X. Zhang, W.L. Hase, M. Weidemuller and R. Wester, *Science*, 2008, **319**, 183.
[107] C.K. Ni and Y.T. Lee, *Int. Rev. Phys. Chem.*, 2004, **23**, 187.
[108] S.T. Tsai, C.K. Lin, Y.T. Lee and C.K. Ki, *Rev. Sci. Instrumen.,* 2001, **72**, 1963.
[109] M.H. Kim, B.D. Leskiw, and A.G. Suits, *J. Phys. Chem. A*, 2005, **109**, 7839.
[110] C. Vallance and M. Brouard, private communication (2009).
[111] A. Stolow and J.G. Underwood, *Adv. Chem. Phys.*, 2008, **139**, 497.
[112] T. Suzuki, *Annu. Rev. Phys. Chem.*, 2006, **57**, 555.
[113] S. Buelow, G. Radhakrishnan, J. Catanzarite and C. Wittig, *J. Chem. Phys.*, 1985, **83**, 444.
[114] S. Buelow, M. Noble, G. Radhakrishnan, H. Reisler, C. Wittig and H. Hancock, *J. Phys. Chem.*, 1986, **90**, 1015.
[115] C. Jouvet and B. Soep, *Chem. Phys. Lett.*, 1983, **96**, 426.
[116] C. Jouvet and B. Soep, *J. Chem. Phys.*, 1984, **80**, 2229.
[117] N.F. Scherer, L.R. Khundkar, R.B. Bernstein and A.H. Zewail, *J. Chem. Phys.*, 1987, **87**, 1451.
[118] D. Raftery, E. Gooding, A. Romanovsky and R.M. Hochstrasser, *J. Chem. Phys.*, 1994, **101**, 8572.
[119] D. Raftery, M. Iannone, C.M. Phillips and R.M. Hochstrasser, *Chem. Phys. Lett.*, 1993, **201**, 513.
[120] L. Sheps, A.C. Crowther, S.L. Carrier and F.F. Crim, *J. Phys. Chem. A*, 2006, **110**, 3087.
[121] L. Sheps, A.C. Crowther, C.G. Elles and F.F. Crim, *J. Phys. Chem. A*, 2005, **109**, 4296.
[122] C.G. Elles, F.F. Crim, *Annu. Rev. Phys. Chem.*, 2006, **57** 273.
[123] A.C. Crowther, S.L Carrier, T.J. Preston and F.F. Crim, *J. Phys. Chem. A*, 2008, **112**, 12081.
[124] A.C. Crowther, S.L Carrier, T.J. Preston and F.F. Crim, *J. Phys. Chem. A*, 2009, **113**, 3758.

Figure 1

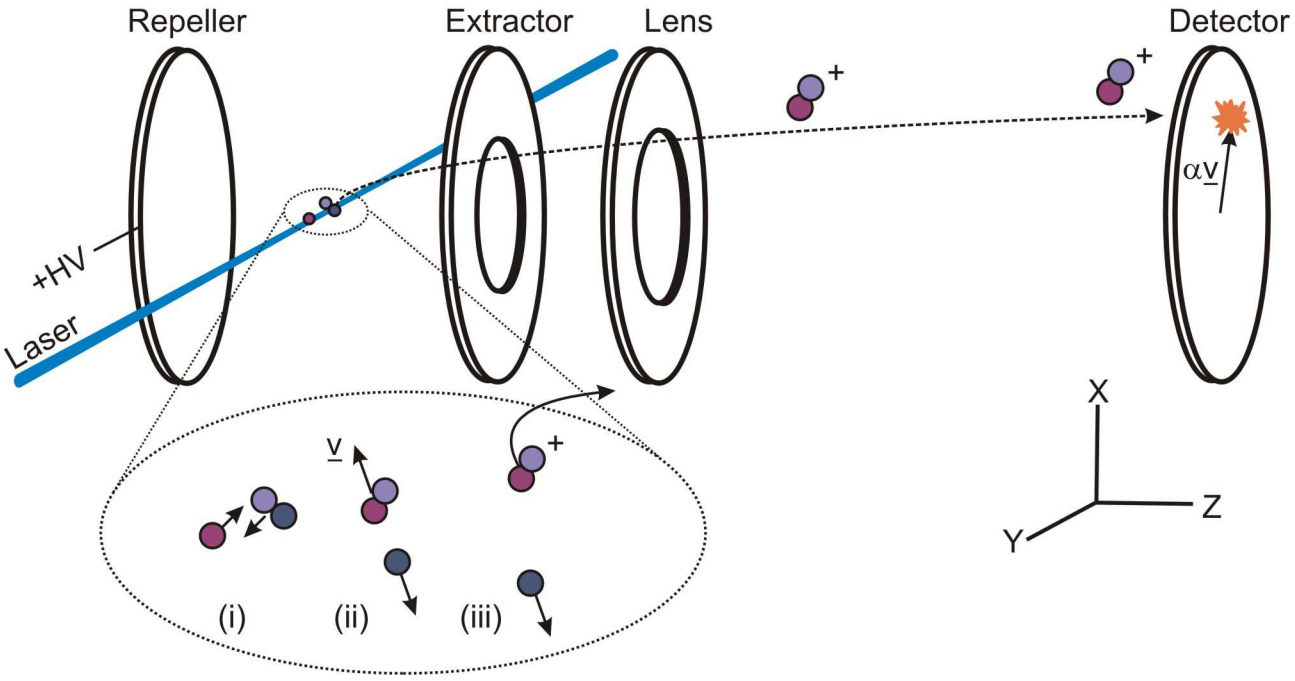

Figure 2

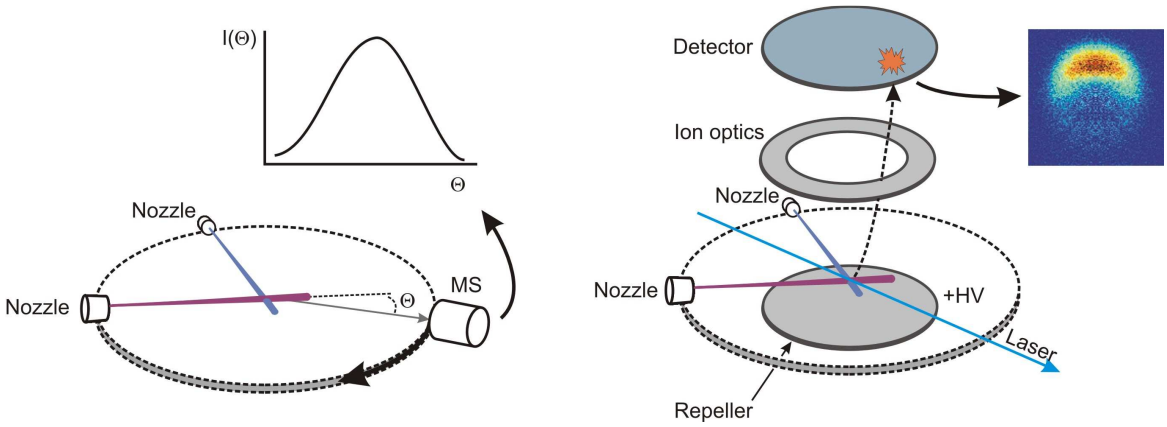
I(Θ)
Θ
Nozzle
Nozzle
MS
Θ
Detector
Ion optics
Nozzle
Nozzle
+HV
Laser
Repeller

Figure 3

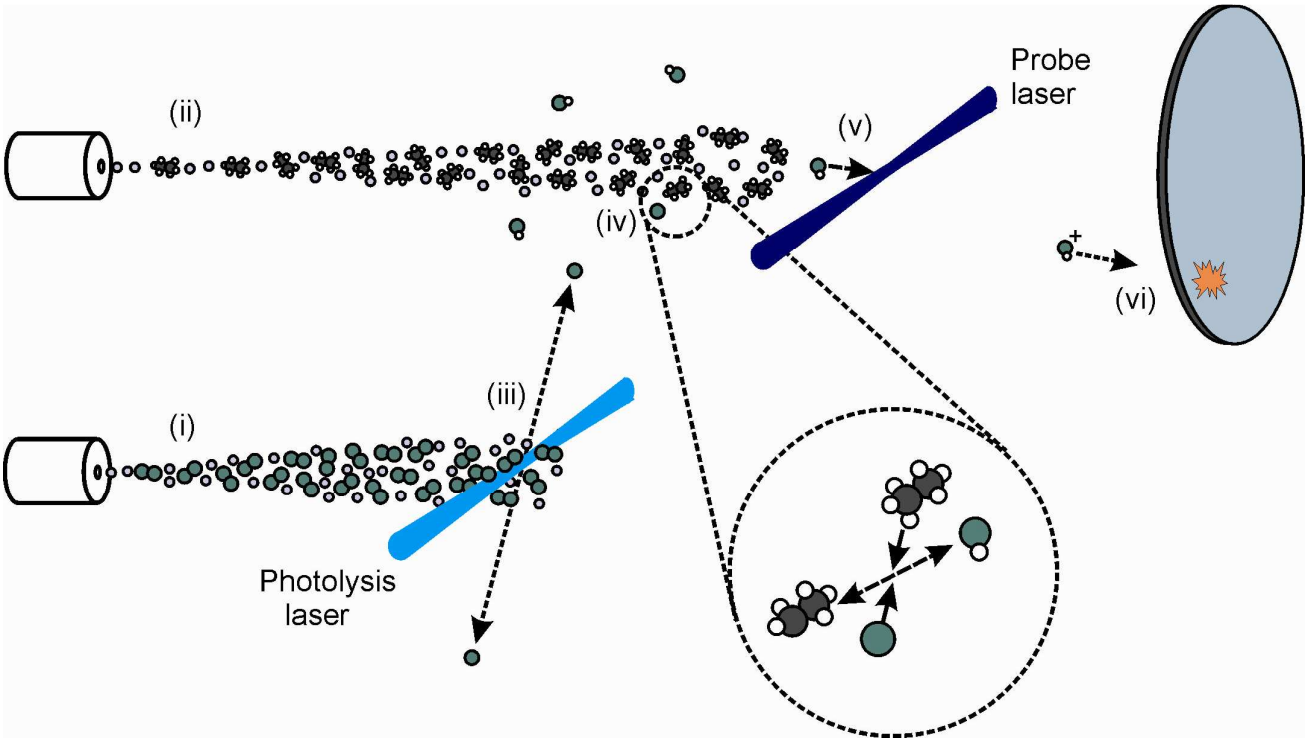

Figure 4

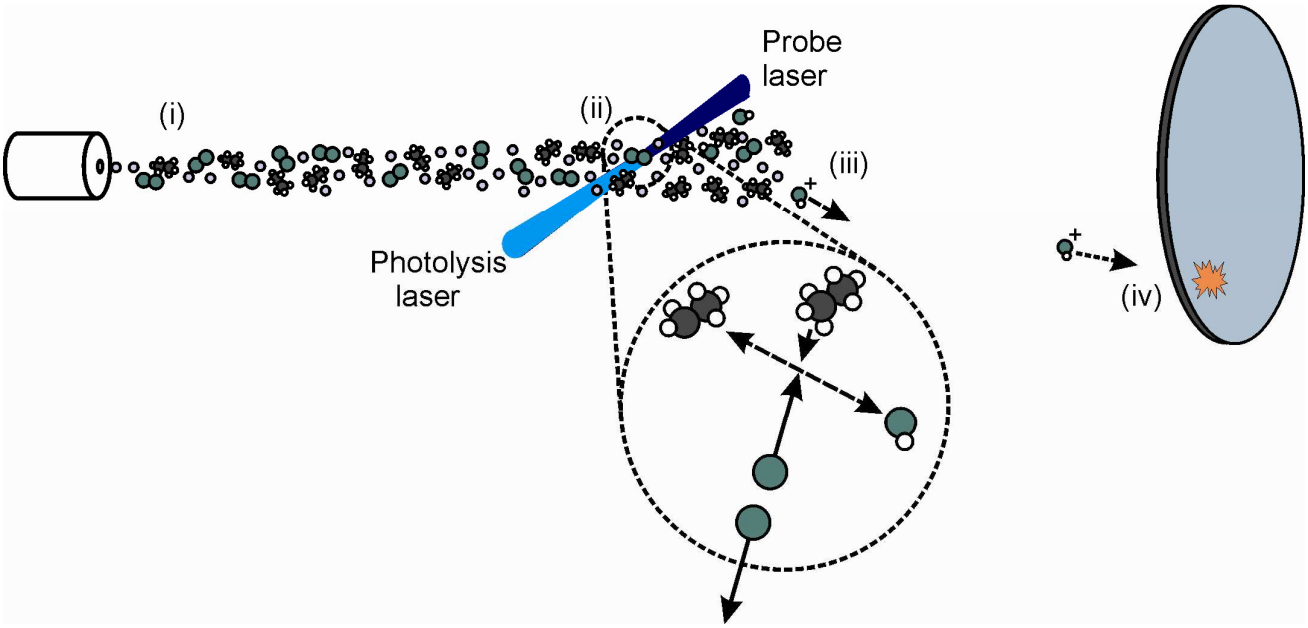

Figure 5

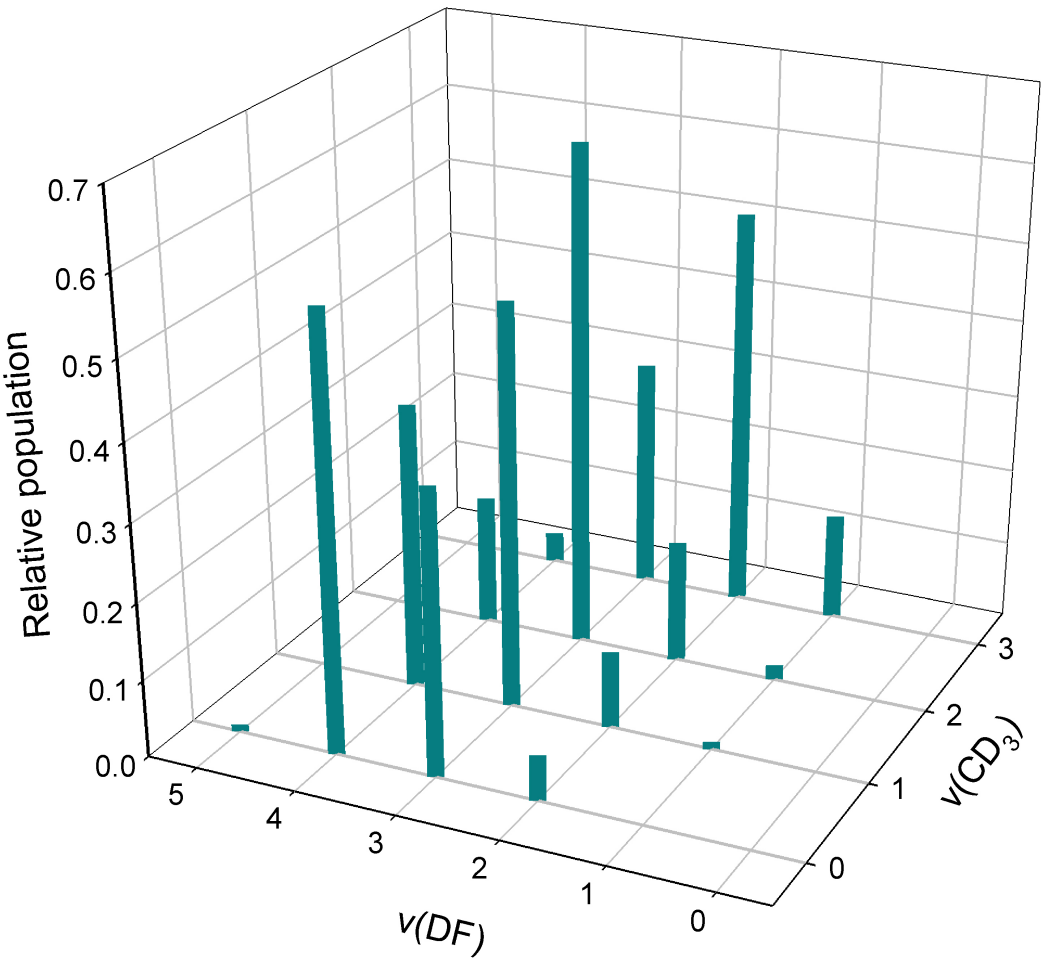
Relative population
0.0
0.1
0.2
0.3
0.4
0.5
0.6
0.7
v(DF)
5
4
3
2
1
0
v(CD3)
0
1
2
3

Figure 6

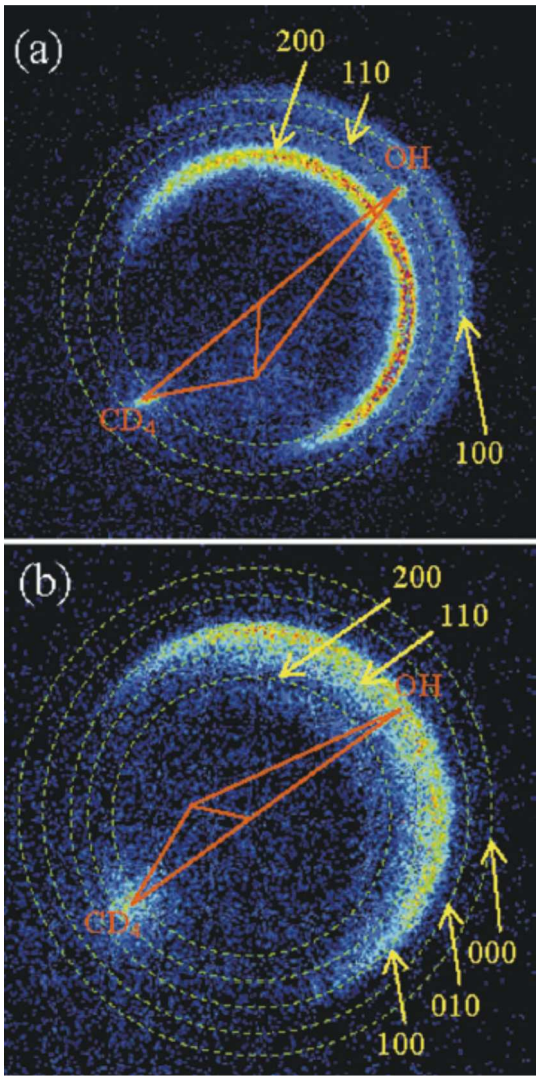

Figure 7

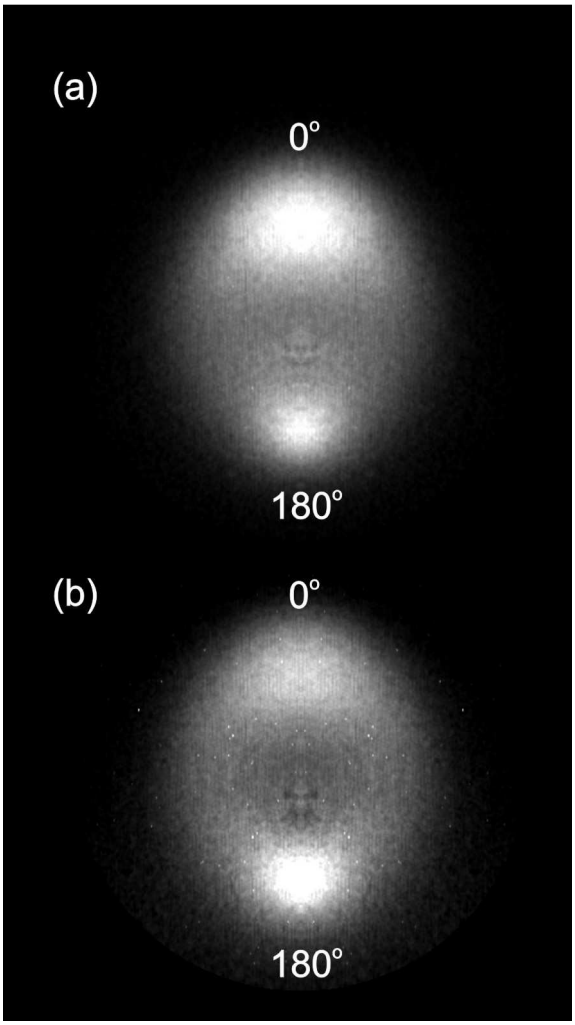

Figure 8

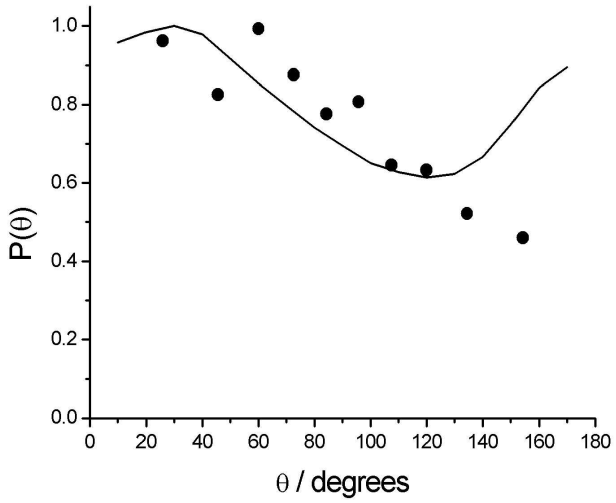

Figure 9

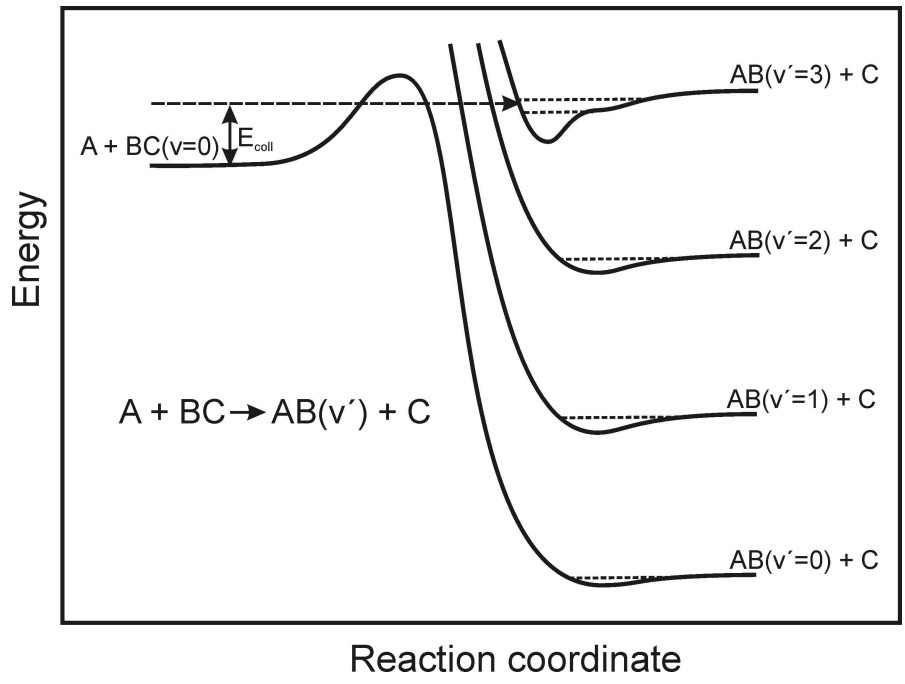
Energy
A + BC(v=0)
E_{coll}
A + BC → AB(v´) + C
AB(v´=3) + C
AB(v´=2) + C
AB(v´=1) + C
AB(v´=0) + C
Reaction coordinate

Figure 10

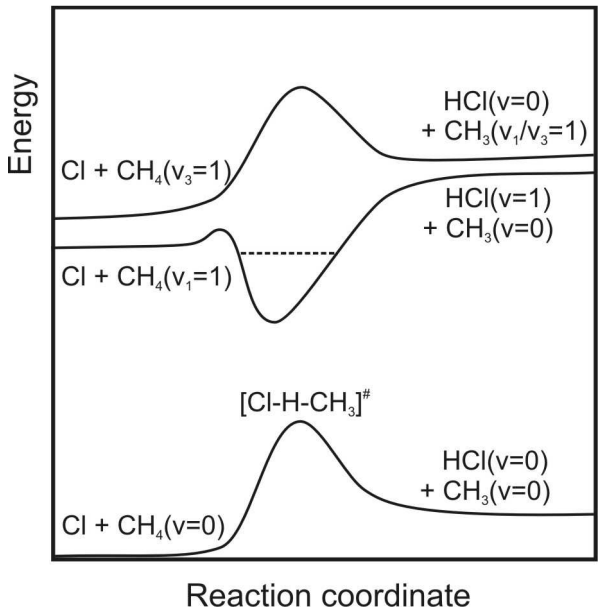
Energy
Cl + CH4(v3=1)
HCl(v=0)
+ CH3(v1/v3=1)
HCl(v=1)
+ CH3(v=0)
Cl + CH4(v1=1)
[Cl-H-CH3]#
HCl(v=0)
+ CH3(v=0)
Cl + CH4(v=0)
Reaction coordinate